

Transport analysis of K^+ production in proton-nucleus reactions

Z. Rudy¹, W. Cassing², L. Jarczyk¹, B. Kamys¹, A. Kowalczyk^{1,2}, and P. Kulesa³

¹ M. Smoluchowski Institute of Physics, Jagellonian University, PL-30059 Cracow, Poland

² Institut für Theoretische Physik, Justus Liebig Universität Giessen, D-35392 Giessen, Germany

³ W. Niewodniczański Institute of Nuclear Physics, PL-31342, Cracow, Poland

Received: date / Revised version: date

Abstract. The production of K^+ mesons in proton-nucleus collisions from 1.0 to 2.3 GeV is analyzed with respect to one-step nucleon-nucleon ($NN \rightarrow NYK^+$) and two-step Δ -nucleon ($\Delta N \rightarrow K^+YN$) or pion-nucleon ($\pi N \rightarrow K^+Y$) production channels on the basis of a coupled-channel transport approach (CBUU) including the kaon final-state-interactions (FSI). Momentum-dependent potentials for the nucleon, hyperon and kaon in the final state are included as well as K^+ elastic rescattering in the target nucleus. The transport calculations are compared to the experimental K^+ spectra taken at COSY-Jülich. Our systematic analysis of K^+ spectra from ^{12}C , ^{63}Cu , ^{107}Ag and ^{197}Au targets as well as their momentum differential ratios gives a repulsive K^+ potential of 20 ± 5 MeV at normal nuclear matter density.

PACS. 13.60.Le Meson production – 13.75.Jz Kaon-baryon interactions – 14.40.Aq Pi, K, and eta mesons – 24.40.-h Nucleon-induced reactions

1 Introduction

The production of heavy mesons in $p+A$ reactions at bombarding energies far below and close to the free nucleon-nucleon threshold is of specific interest [1]-[17] as one hopes to learn either about cooperative nuclear phenomena and/or about high momentum components of the nuclear many-body wave function that arise from nucleon-nucleon correlations. Especially K^+ mesons have been considered as promising hadronic probes [18,19,20] due to the rather moderate final state interaction, which is a consequence of strangeness conservation.

Experiments on K^\pm production from nucleus-nucleus collisions at SIS energies of 1–2 A·GeV have shown that in-medium properties of the kaons are seen in the collective flow pattern of K^+ mesons both, in-plane and out-of-plane, as well as in the abundancy of antikaons [21,22,23]. Thus in-medium modifications of the mesons have become a topic of substantial interest in the last decade triggered in part by the early suggestion of Brown and Rho [24], that the modifications of hadron masses should scale with the scalar quark condensate $\langle q\bar{q} \rangle$ at finite baryon density.

As demonstrated in the pioneering work of Kaplan and Nelson [25,26] kaons and antikaons couple attractively to the scalar nucleon density with a strength proportional to the $KN - \Sigma$ constant Σ_{KN} , which is not well known at present and may vary from 270 to 450 MeV. Furthermore, a vector coupling to the quark 4-current – for vanishing spatial components – leads to a repulsive potential term for the kaons and to an additional attractive term for the antikaons. In fact, the recent observation of a rather

narrow strange tribaryon state with mass 3.115 GeV in Ref. [27] – observed in the $^4He(K^-, p)X$ reaction with antikaons at rest – has given further experimental evidence for strong attractive K^- potentials in (light) nuclei.

Nevertheless, the actual kaon and antikaon self energies (or potentials) at normal nuclear matter density (and above) are quite a matter of debate – due to higher order terms in the chiral expansion – especially for the antikaon [28,29,30]. Moreover the momentum-dependence of their self energies is widely unknown (except for a dispersion analysis in Ref. [31]) since most Lagrangian models are restricted to s -wave interactions or only include additional p -waves. It is thus mandatory to perform experimental studies of the (anti-) kaon properties under well controlled conditions, e.g. in proton-nucleus reactions, where one probes the (anti-) kaon self energies at normal nuclear matter density $\rho_0 \approx 0.16 \text{ fm}^{-3}$ and below. Furthermore, by gating on kaon momenta in the laboratory, one might be able to obtain information on the momentum dependence of the self energies, too.

K^+ production in $p+A$ collisions at subthreshold energies has been observed experimentally more than a decade ago by Koptev et al. [19] at bombarding energies from 0.8 to 1.0 GeV. However, only total K^+ yields could be extracted at that time at subthreshold energies. In more recent years differential K^+ spectra have been measured down to 1.2 GeV for ^{12}C targets at 40° [32] (SATURNE) or 90° in the laboratory [33] (CELSIUS). Unfortunately, the different experiments have no overlap in acceptance and the interpretation of the data, if compatible at all, remains vague [14,34]. First data on the full momentum

distribution at forward angles have been presented by the ANKE Collaboration at COSY-Jülich [35] for K^+ mesons from $p + {}^{12}\text{C}$ reactions at 1.0 GeV in 2001 [36] and at higher bombarding energies in the last year [37].

In this study we use the coupled-channel (CBUU) transport model that has been developed first in Ref. [38] for the description of nucleus-nucleus collisions and later on employed for the simulation of pion- and proton-nucleus reactions [31, 39, 40], too. For applications to K^\pm production in nucleus-nucleus collisions at SIS energies we refer the reader to Refs. [41]. In this model the effects of momentum-dependent self energies for all hadrons can be studied explicitly as well as their production and propagation in the nuclear medium. The actual version of the CBUU transport model employed in our present analysis is identical to that described in Ref. [34]. We thus discard an explicit description and refer the reader to Ref. [34] for technical details and the explicit momentum-dependent potentials employed for the nucleon and hyperon degrees of freedom.

The paper is organized as follows: We very briefly recapitulate the concepts of the CBUU model in Section 2 and step on with the actual results for K^+ spectra in $p + A$ collisions at COSY energies in Section 3 in comparison to the data of the ANKE collaboration [37]. In Section 4 we compare the calculated ratios of K^+ spectra for different kaon potentials with the corresponding data at various bombarding energies [37]. This systematic analysis will lead to an approximate extraction of the strength of the K^+ potential in the nuclear medium. A summary concludes this paper in Section 5.

2 Brief reminder of the CBUU transport model

In this work we perform our analysis along the line of the CBUU¹ approach [38] which is based on a coupled set of transport equations for the phase-space distributions $f_h(x, p)$ of hadron h , i.e. [42]

$$\begin{aligned} & (\Pi_\mu - \Pi_\nu \partial_\mu^p U_h^\nu - M_h^* \partial_\mu^p U_h^S) \partial_x^\mu f_h(x, p) \\ & + (\Pi_\nu \partial_\mu^x U_h^\nu + M_h^* \partial_\mu^x U_h^S) \partial_p^\mu f_h(x, p) \\ & = \sum_{h_2 h_3 h_4 \dots} \int d^2 d^3 d^4 [G^\dagger G]_{12 \rightarrow 34 \dots} \\ & \quad \times \delta^4(\Pi + \Pi_2 - \Pi_3 - \Pi_4) \\ & \quad \times \{ f_{h_3}(x, p_3) f_{h_4}(x, p_4) \bar{f}_h(x, p) \bar{f}_{h_2}(x, p_2) \\ & \quad - f_h(x, p) f_{h_2}(x, p_2) \bar{f}_{h_3}(x, p_3) \bar{f}_{h_4}(x, p_4) \} . \end{aligned} \quad (1)$$

In Eq. (1) $U_h^S(x, p)$ and $U_h^\mu(x, p)$ denote the real part of the scalar and vector hadron selfenergies, respectively, while $[G^\dagger G]_{12 \rightarrow 34 \dots} \delta^4(\Pi + \Pi_2 - \Pi_3 - \Pi_4 \dots)$ is the 'transition rate' for the process $1 + 2 \rightarrow 3 + 4 + \dots$ which is taken to be on-shell in the semiclassical limit adopted. The hadron

quasi-particle properties in (1) are defined via the mass-shell constraint

$$\delta(\Pi_\mu \Pi^\mu - M_h^{*2}) , \quad (3)$$

with effective masses and momenta (in local Thomas-Fermi approximation) given by [42]

$$\begin{aligned} M_h^*(x, p) &= M_h + U_h^S(x, p) \\ \Pi^\mu(x, p) &= p^\mu - U_h^\mu(x, p) , \end{aligned} \quad (4)$$

while the phase-space factors

$$\bar{f}_h(x, p) = 1 \pm f_h(x, p) \quad (5)$$

are responsible for fermion Pauli-blocking or Bose enhancement, respectively, depending on the type of hadron in the final/initial channel. The transport approach (1) is fully specified by $U_h^S(x, p)$ and $U_h^\mu(x, p)$ ($\mu = 0, 1, 2, 3$), which determine the mean-field propagation of the hadrons, and by the transition rates $G^\dagger G \delta^4(\dots)$ in the collision term (5), that describes the scattering and hadron production/-absorption rates.

The scalar and vector mean fields U_h^S and U_h^μ for nucleons are modeled in line with Ref. [43] and presented explicitly in Fig. 1 of Ref. [34] for the resulting real part of the nucleon potential $U_N(p)$. We recall that this nucleon potential (at density ρ_0) is attractive for momenta p below 0.6 GeV/c and repulsive above. Apart from the nuclear potentials each charged hadron additionally moves in the background of the Coulomb potential that is generated by the charged hadrons themselves. In case of proton-nucleus reactions – with the nucleus at rest – this essentially amounts to a Coulomb acceleration in the final state for positively charged hadrons and a deceleration for negatively charged particles. Note, that for heavy nuclei like Pb or Au the Coulomb potential in the nuclear interior (for p, π^+, K^+) is ~ 20 MeV, i.e. of the same order of magnitude as the 'expected' repulsive K^+ nuclear potential [34, 44].

The hyperon mean fields, furthermore, are assumed to be 2/3 of the nucleon potentials. In the present approach, apart from nucleons, $\Delta, N(1440), N(1535), \Lambda, \Sigma$ with their isospin degrees of freedom, we propagate explicitly pions, K^+ , and η 's and assume that the pions as Goldstone bosons do not change their properties in the medium. The kaon potential is taken as momentum independent (cf. Ref. [34]), while its strength is varied in the dynamical calculations from 0 to 20 MeV at nuclear matter density ρ_0 assuming a linear increase with the actual nucleon density $\rho(\mathbf{r})$.

The calculation of 'subthreshold' particle production is treated perturbatively in the energy regime of interest due to the small cross sections involved. Since we work within the parallel ensemble algorithm in the CBUU approach, each parallel run of the transport calculation can be considered approximately as an individual reaction event, where binary reactions in the entrance channel at given invariant energy \sqrt{s} lead to final states with 2 (e.g. K^+Y in πB channels), 3 (e.g. for K^+YN channels in BB

¹ Coupled-Channel Boltzmann-Uehling-Uhlenbeck

collisions) or 4 particles (e.g. $K\bar{K}NN$ in BB collisions) with a relative weight P_i for each event i which is defined by the ratio of the production cross section to the total hadron-hadron cross section. We thus dynamically gate on all events where a K^+ meson is produced initially. Each strange hadron production event i is represented by $\sim 10^3$ testparticles for the final strange hadron j with individual weight W_j^i such that the sum of the weights W_j^i over j reproduces the individual production probability P_i and the distribution in momenta (multiplied with the NN or πN cross section) describes the differential production cross section (cf. Ref. [34] for details).

For the present study the production of pions by pN collisions in $p + A$ reactions as well as the total kaon cross sections in pN and πN collisions are of relevance. The pion production cross section from NN interactions is based on the parametrization of the experimental data by Ver West and Arndt [45] and implemented in the transport model as described in Ref. [38]. The cross sections for the channels $\pi N \rightarrow KY$, where Y stands for a hyperon Λ, Σ , are taken from the analysis of Huang et al. [46] and essentially correspond to the experimental data for the different πN channels in vacuum (or 'free' space). Note, that in addition to the early studies in [16,17] the channels with a Σ hyperon are taken into account. All cross sections are reparametrized as a function of the invariant energy above threshold $\sqrt{s} - \sqrt{s_0}$ [21], where $\sqrt{s_0}$ denotes the threshold for the individual channel given by the sum of the hadron masses in the final state of the reaction. We recall that the differential cross sections for binary reactions are fully determined by the total cross sections when assuming S -wave dominance.

The question arises, furthermore, about the in-medium production cross sections - essentially at density ρ_0 - if potentials or self energies are involved. Here we employ the assumption that the production matrix element squared $|M|^2$ does not change in the medium and the change of cross section can be described by a change of the available phase space. This notion is guided by the experimental observation that meson production from pp collisions is well described by phase space [47] if final state interactions (FSI) between the hadrons are taken into account. These FSI, furthermore, are found to be dominated by the final baryon-baryon interaction, which is very strong in the pp, pn or $p\Lambda$ channels in free space. On the other hand, such FSI's are screened in the nuclear medium due to the surrounding nucleons such that in-medium production cross sections for mesons are expected to vary essentially with the available phase space. It is thus sufficient to shift the threshold in a pN collision to

$$\sqrt{s_0^*} = \Pi_N^0(p_N) + \Pi_\Lambda^0(p_\Lambda) + \Pi_K^0(p_K) \quad (6)$$

using (4), where the momenta p_j denote the relative momenta with respect to the nuclear matter rest frame and $\Pi_j^0(p)$ is the energy of hadron j including the potentials (4).

3 Comparison to experimental spectra

In this Section we show the influence of nucleon and kaon potentials on K^+ spectra from $p + {}^{12}\text{C}$ and $p + {}^{197}\text{Au}$ reactions and compare our calculations to the experimental K^+ spectra available from 1.0 GeV – 2.3 GeV bombarding energy from the ANKE collaboration [37] that has taken K^+ spectra in forward direction for $\theta_{lab} \leq 12^\circ$ up to momenta of ~ 500 MeV/c.

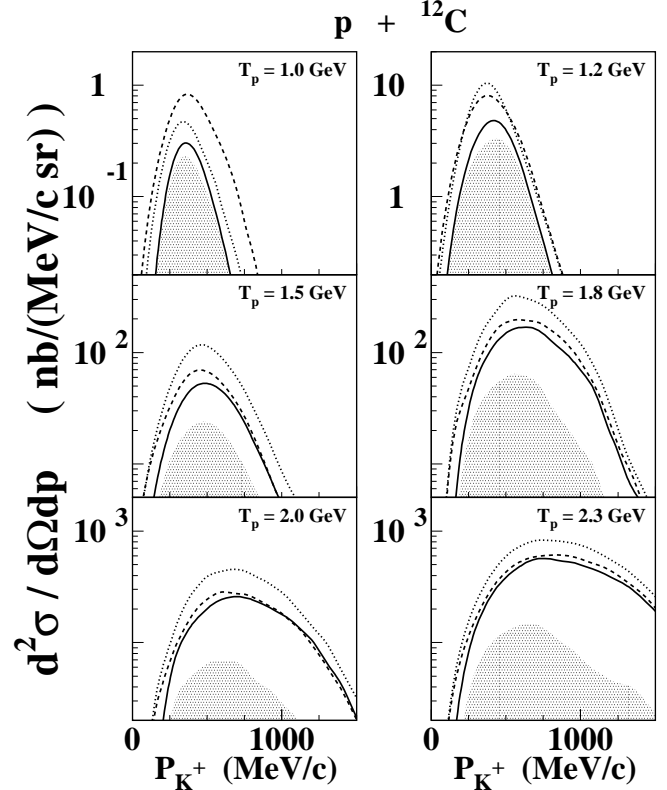


Fig. 1. The calculated differential K^+ spectra for $p + {}^{12}\text{C}$ from 1.0 to 2.3 GeV for $\theta_{lab} \leq 12^\circ$. The dotted line is obtained from CBUU calculations without baryon and kaon potentials, the dashed line shows the results with baryon potentials included while the solid line corresponds to calculations including both, nucleon and kaon potentials (+20 MeV at nuclear density ρ_0). The shaded areas indicates the contributions from the two-step mechanisms $pN \rightarrow \Delta N, \Delta N \rightarrow K^+ Y N$ and $pN \rightarrow \pi NN, \pi N \rightarrow K^+ Y$, respectively, for the case of nucleon and kaon potentials, such that the difference to the solid line corresponds to the primary pN production channel.

The calculated differential K^+ spectra for $p + {}^{12}\text{C}$ from 1.0 GeV to 2.3 GeV for $\theta_{lab} \leq 12^\circ$ are displayed in Fig. 1 and for $p + {}^{197}\text{Au}$ in Fig. 2. The dotted lines are obtained from CBUU calculations without baryon and kaon potentials, the dashed lines show the results with baryon potentials included while the solid lines correspond to calculations with both, nucleon and kaon potentials. In the latter case we have assumed a kaon potential of +20 MeV at density ρ_0 . At the low bombarding energy of 1.0 GeV the nuclear potential in the final state is dominantly at-

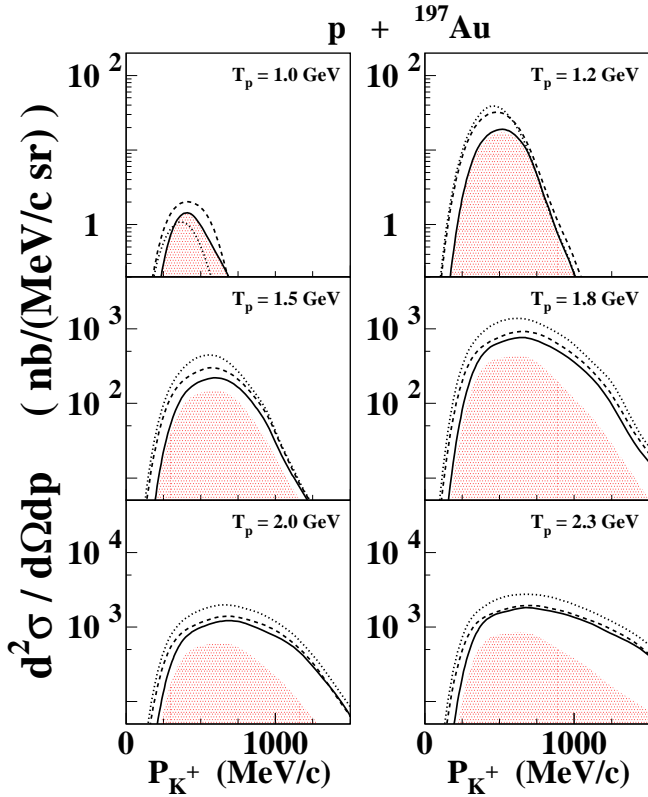


Fig. 2. The same as Fig. 1 for $p + Au$ reactions from 1.0 to 2.3 GeV bombarding energy.

tractive and we obtain an enhancement of the K^+ yield by about a factor of 2 – relative to the calculations without nuclear potential – whereas the additional repulsive K^+ potential leads again to a decrease by a factor ~ 2 -3. For 1.2 GeV the net effect of the nucleon potential is close to zero; its repulsion in the final state for higher bombarding energies becomes visible in a reduction of the K^+ spectrum relative to the ‘free’ case. On the other hand the effect of the repulsive kaon potential is always a reduction of the K^+ spectra, which is most pronounced at very low bombarding energies – when comparing the solid lines relative to the dashed lines – and becomes small at high bombarding energies.

The shaded areas in Figs. 1 and 2 indicate the contributions from the two-step mechanisms $pN \rightarrow \Delta N$, $\Delta N \rightarrow K^+ Y N$ and $pN \rightarrow \pi N N$, $\pi N \rightarrow K^+ Y$, respectively, for the case of nucleon and kaon potentials included (solid line). Thus the role of secondary (Δ and pion induced) reaction channels is clearly visible from Figs. 1 and 2 by comparing the shaded area to the solid line, that correspond to the total spectra. At $T_{lab} = 1.0$ GeV the dominant fraction of the K^+ yield is due to the secondary channels in line with the earlier calculations in Refs. [16,17]. Consequently, one does not probe high momentum components of the nuclear wave function by K^+ spectra in a direct way. However, with increasing bombarding energy the role of the two-step reactions diminishes gradually. At $T_{lab} = 2.3$ GeV the secondary channels in case of a Au target amount to about 30% and in case of a C target

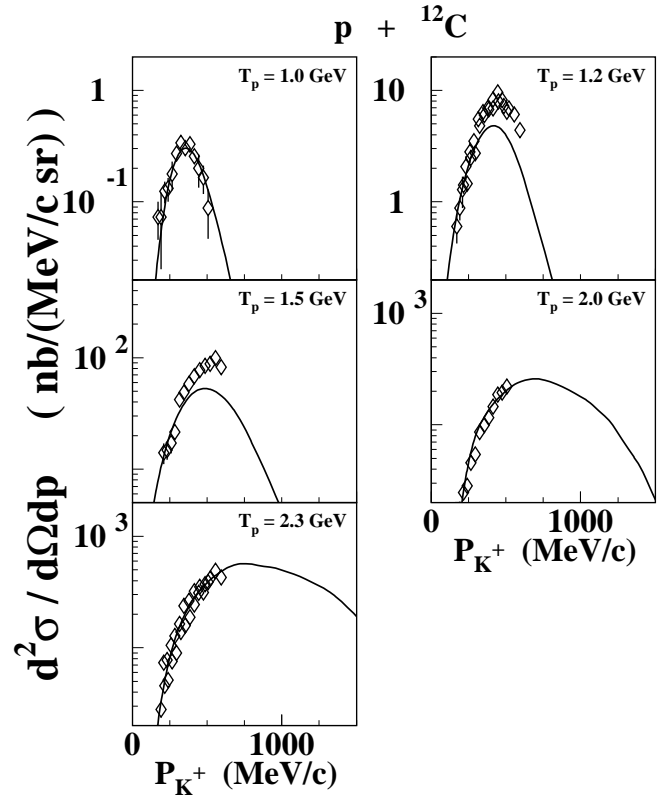


Fig. 3. Comparison of the K^+ spectra from the CBUU calculations (solid lines) with the data from the ANKE collaboration [36,37] for $p + {}^{12}C$. The calculations include both the momentum-dependent nucleon potential as well as a repulsive K^+ potential of +20 MeV at density ρ_0 .

to less than 20%. This relative change with target mass number is attributed to the fact that for the small ${}^{12}C$ target only a fraction of the high energy pions rescatters in the target and produces $K^+ Y$ pairs. Moreover, the role of the secondary channels decreases with increasing kaon momentum such that the high momentum tail of the K^+ spectra is dominated by the first chance pN production channel in line with the studies by Paryev [48].

How do these calculations compare to the data from the ANKE collaboration [36,37] and what can we learn from that? To answer this question we show in Fig. 3 our calculations that include the baryon and K^+ potentials (solid lines) with the measured spectra for $p + {}^{12}C$ from Refs. [36,37]. Whereas the description of the experimental spectrum looks almost perfect at 1.0 GeV the data are slightly underestimated at $T_{lab} = 1.2$ and 1.5 GeV in the maximum. At these energies the maximum of the spectrum is better described without kaon and nuclear potentials, but then the spectra no longer match in the low momentum part. Thus a repulsive K^+ potential is needed to properly describe the shape of the spectrum especially for low momenta. On the other hand, channels such as $pN_1 \rightarrow d + \pi$ followed by a secondary reaction $\pi + N_2 \rightarrow K^+ + Y$ are not included in the present transport calculations. Such channels have been found in Ref. [49] to contribute to the kaon spectrum at bombarding

energies ~ 1.2 GeV but to be insignificant at higher energies of 2.0 to 2.3 GeV. As can be seen from Fig. 3 the calculations – including nucleon and kaon potentials – are in a good agreement with the experimental spectra again at 2.0 and 2.3 GeV which is in line with the findings of Ref. [49].

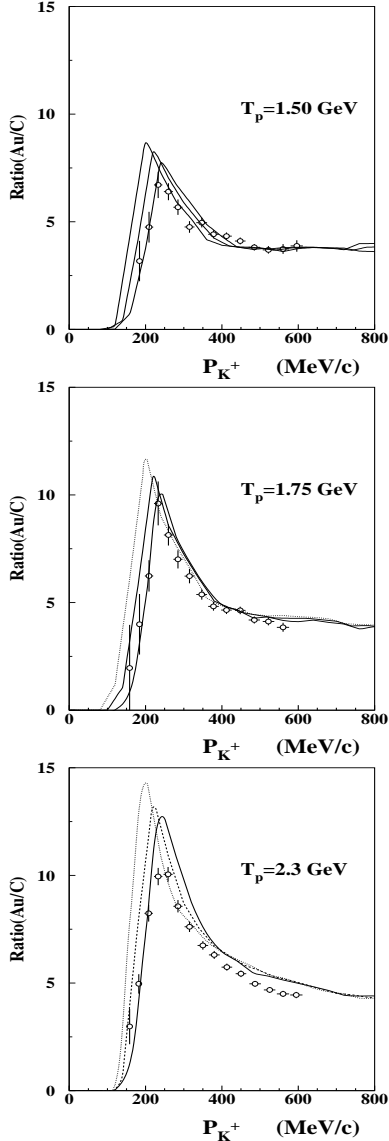


Fig. 4. The ratio of the calculated differential K^+ spectra from $p + Au$ to $p + C$ reactions at 1.5, 1.75 and 2.3 GeV in comparison to the data from Ref. [37]. The different solid lines correspond to calculations employing different kaon potentials at normal nuclear density ρ_0 . Starting from the left the results correspond to repulsive kaon potentials of 0, 10 and 20 MeV at ρ_0 .

4 K^+ spectral ratios

The differential K^+ momentum spectra in Figs. 1 to 3 differ in their low momentum part – at fixed bombarding energy – when varying the target mass number. In Refs. [34, 44] it has been pointed out that the variation in the low K^+ momentum spectrum is a consequence of i) the different acceleration of the charged kaon in the Coulomb field of the target and ii) an additional acceleration in the repulsive kaon potential in the nuclear medium (target nucleus). The combined effect of both the Coulomb and nuclear repulsion is most easily seen when comparing the K^+ spectra from different targets. To this aim we show in Fig. 4 the ratio of the spectra from Au to C targets at 1.5, 1.75 and 2.3 GeV, where this effect is most pronounced (cf. Ref. [44]). The different solid lines in Fig. 4 correspond to calculations employing different nuclear kaon potentials of magnitude 0, 10 and 20 MeV at normal nuclear density ρ_0 (starting from the left).

It is seen that the ratio for (Au/C) is approximately independent on the bombarding energy and shows a maximum at about 230 MeV/c. When neglecting kaon repulsion from nuclear forces – including only Coulomb repulsion – this maximum shows up slightly below 200 MeV/c, which is clearly too low in comparison to the data (cf. [37, 44]). We recall that the relative strength of the momentum shift in the forward K^+ spectra is proportional to the square root of the sum of Coulomb and nuclear potentials,

$$\Delta p \approx \sqrt{2M_K(U_{Coul} + U_K)}, \quad (7)$$

which implies that an additional repulsive nuclear K^+ potential is needed to describe the data. Since the strength of this potential – linear in the nuclear density at the K^+ production point – is a ‘parameter’ in the transport calculations, we may in turn determine the strength of this potential in comparison to the data. A χ^2 -fit gives $U_K(\rho_0) \approx 20 \pm 5$ MeV for the ratio of $p + Au$ to $p + C$ reactions.

We mention that the transport calculations have a limited accuracy due to low statistics in some regions of phase space. This holds true especially for the low momentum spectrum of the kaons in the acceptance of the ANKE spectrometer and has an impact also on the ratio of the spectra from different targets. In the χ^2 -fit addressed above the statistical inaccuracy of the calculations has been included.

It is of further interest whether the interpretation of the momentum differential kaon spectrum – discussed above – is compatible with the ratios from other targets, too. To this aim we show in Fig. 5 the same ratios as in Fig. 4 but for Ag/C and Cu/C at 2.3 GeV in comparison to the data from Ref. [37]. It is clearly seen that the experimental ratios are consistent with the transport calculations for $U_K(\rho_0) = +20$ MeV though the sensitivity to the strength of the kaon potential is reduced. This is basically due to the fact that the surface area – relative to the total volume – of the lighter targets is larger than for the heavy Au nucleus.

Nevertheless, the agreement between the CBUU calculations and the data is remarkable and demonstrates that the underlying K^+ dynamics is rather well understood.

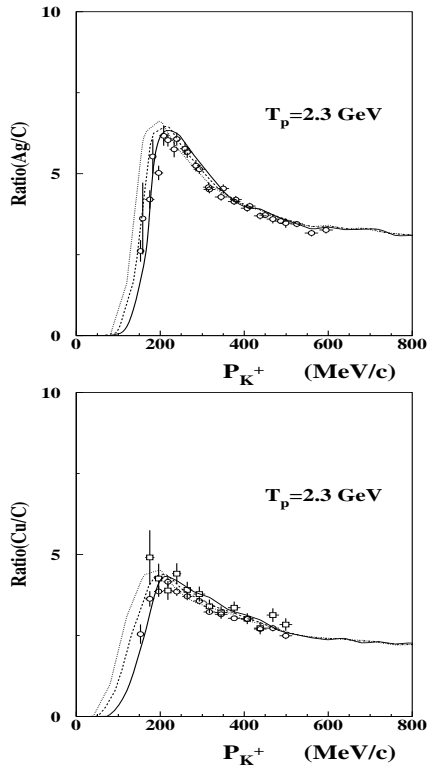


Fig. 5. The same ratios as in Fig. 4 but for Ag/C and Cu/C at 2.3 GeV in comparison to the data from Ref. [37].

5 Summary

In this work we have studied the production of K^+ mesons in proton-nucleus collisions from 1.0 to 2.3 GeV with respect to one-step nucleon-nucleon and two-step Δ -nucleon or pion-nucleon production channels on the basis of a coupled-channel transport approach (CBUU) including differential transition probabilities from πN reactions (cf. Ref. [34]). We have included the kaon final state interactions, which are important for heavy targets, and incorporated the effects of momentum-dependent potentials for the nucleon, hyperon and kaon in the nucleus. A comparison of the calculations to the experimental K^+ spectra taken at COSY-Jülich has shown that the momentum differential K^+ yield can be reproduced in magnitude and shape within an accuracy better than 30% at all bombarding energies.

The detailed calculations have demonstrated that the spectra show a substantial sensitivity to the potentials and their momentum dependence. At low bombarding energies of ~ 1.0 GeV the net attractive potentials for the nucleon and the Λ -hyperon in the final state lead to a relative enhancement of the K^+ spectra while at higher bombarding energies (~ 2 GeV) the baryon potentials are repulsive and thus suppress K^+ production relative to the free case. This phenomenon is seen in the excitation function of the K^+ cross section when varying T_{lab} from 1.0 – 2.3 GeV (cf. Fig. 3). Furthermore, the shape of the spectrum for low K^+ momenta in the laboratory is very sensitive to both, Coulomb and nuclear kaon potentials, since

the kaons are accelerated by both forces when leaving the nuclear environment and propagating to the continuum. The relative strength of this momentum shift in the forward K^+ spectra is proportional to the square root of the sum of both potentials (7). Thus the K^+ spectral shape at low momenta (or kinetic energies T_K) allows to determine the strength of the K^+ potential from experimental data in an almost model independent way especially when comparing kaon spectra from light and heavy targets at the same bombarding energy (cf. Refs. [37, 44, 50]). In fact, the shape of such ratios is practically independent of bombarding energy but sensitive to the strength of the kaon repulsion in the medium. Our systematic study has given a value of 20 ± 5 MeV at normal nuclear density ρ_0 which agrees with the result from the scattering length approximation [29].

We point out that our calculations slightly underpredict the spectra at 1.2 and 1.5 GeV indicating that additional reaction channels should be at work which have not been included in the CBUU calculations. In fact, the experimental studies by the ANKE collaboration in Ref. [49] have shown that there is an additional K^+ production from the secondary channel $p + N_1 \rightarrow d + \pi$; $\pi + N_2 \rightarrow K^+ + \Lambda$ at a bombarding energy of 1.2 GeV in $p + C$ reactions. However, no signals for this channel have been seen at higher bombarding energies of ~ 2 GeV. This interpretation is well in line with our present transport calculations since the description of the available spectra at 2.0 and 2.3 GeV for $p + {}^{12}C$ implies that further reaction channels do not contribute significantly at the higher bombarding energy. It remains presently an open question whether a cooperative production mechanism by two- or three-nucleon clusters – not included in our transport calculations – might contribute and be identified from the experimental side in $p + A$ reactions at very low energies.

The authors like to acknowledge valuable discussions with M. Büscher, V. Koptev, M. Nikipelov, P. Senger, A. Sibirtsev, H. Ströher and C. Wilkin on various issues of this study.

References

1. P. Grimm, E. Grosse, Prog. Part. Nucl. Phys. **15**, 339 (1985)
2. P. Braun-Munzinger, J. Stachel, Ann. Rev. Nucl. Part. Sci. **37**, 1 (1987)
3. J. Randrup, C. M. Ko, Nucl. Phys. A **343**, 519 (1980); A **411**, 537 (1983)
4. J. Cugnon, R. M. Lombard, Nucl. Phys. A **422**, 635 (1984)
5. S. V. Efmov, M. V. Kazarnovsky, E. Ya. Paryev, Z. Phys. A **344**, 181 (1992)
6. V. I. Komarov et al., Nucl. Phys. A **326**, 397 (1979)
7. M. M. Nesterov, N. A. Tarasov, Sov. Phys. JETP **59**, 226 (1984)
8. N. A. Tarasov, V. P. Koptev, M. M. Nesterov, Pis'ma Zh. Eksp. Teor. Fiz. **43**, 217 (1986)
9. H. Müller, Z. Phys. A **339**, 409 (1991); H. Müller, K. Sistemich, Z. Phys. A **344**, 197 (1992)

10. J. Cugnon, P. Deneye, J. Vandermeulen, Phys. Rev. C **41**, 1339 (1990)
11. A. Sibirtsev, M. Büscher, Z. Phys. A **347**, 191 (1994)
12. S. Teis, W. Cassing, T. Maruyama, U. Mosel, Phys. Lett. B **319**, 47 (1993)
13. Yu. T. Kiselev *et al.*, J. Phys. G **25**, 381 (1999).
14. M. Büscher *et al.*, Phys. Rev. C **65**, 014603 (2002).
15. J. Aichelin, C. M. Ko, Phys. Rev. Lett. **55**, 2661 (1985).
16. W. Cassing *et al.*, Phys. Lett. B **238**, 25 (1990)
17. W. Cassing *et al.*, Z. Phys. A **349**, 77 (1994)
18. W. Cassing, V. Metag, U. Mosel, K. Niita, Phys. Rept. **188**, 363 (1990)
19. V. P. Koptev *et al.*, Sov. Phys. JETP **67**, 2177 (1988)
20. J. Geiss, W. Cassing, C. Greiner, Nucl. Phys. A **644**, 107 (1998)
21. W. Cassing, E. L. Bratkovskaya, Phys. Rept. **308**, 65 (1999).
22. Bao-An Li, A. T. Sustich, Bin Zhang, C. M. Ko, Int. Jour. Mod. Phys. E **10**, 267 (2001).
23. P. Senger, Prog. Part. Nucl. Phys. **53**, 1 (2004).
24. G. E. Brown, M. Rho, Phys. Rev. Lett. **66**, 2720 (1991).
25. A.E. Nelsen, D. Kaplan, Phys. Lett. B **192**, 193 (1987).
26. D. B. Kaplan, A.E. Nelson, Phys. Lett. B **175**, 57 (1986).
27. T. Suzuki *et al.*, Phys. Lett. B **597**, 263 (2004).
28. A. Gal, Nucl. Phys. A **691**, 268 (2001).
29. M. Lutz, Phys. Lett. B **426**, 12 (1998).
30. A. Ramos, S. Hirenzaki, S. S. Kamalov, T.T.S. Kuo, Y. Okumura, E. Oset, A. Polls, H. Toki, L. Tolos, Nucl. Phys. A **691**, 259 (2001).
31. A. Sibirtsev, W. Cassing, Nucl. Phys. A **641**, 476 (1998).
32. M. Debowski *et al.*, Z. Phys. A **356**, 313 (1996).
33. A. Badala *et al.*, Phys. Rev. Lett. **80**, 4863 (1998).
34. Z. Rudy *et al.*, Eur. Phys. J. A **15**, 303 (2002)
35. S. Barsov *et al.*, Nucl. Instrum. Methods Phys. Res. A **462**, 364 (2001).
36. V. Koptev *et al.*, Phys. Rev. Lett. **87**, 022301 (2001).
37. M. Büscher *et al.*, nucl-ex/0401031, Eur. Phys. J. A, in print.
38. Gy. Wolf *et al.*, Nucl. Phys. A **517**, 615 (1990); Nucl. Phys. A **552**, 549 (1993).
39. Z. Rudy *et al.*, Z. Phys. A **354**, 445 (1996).
40. Ye. S. Golubeva, L. A. Kondratyuk, W. Cassing, Nucl. Phys. A **625**, 832 (1997).
41. W. Cassing *et al.*, Nucl. Phys. A **614**, 415 (1997); E. L. Bratkovskaya *et al.*, Nucl. Phys. A **622**, 539 (1997).
42. K. Weber *et al.*, Nucl. Phys. A **539**, 713 (1992); T. Maruyama *et al.*, Nucl. Phys. A **573**, 653 (1994).
43. W. Cassing, E. L. Bratkovskaya, S. Juchem, Nucl. Phys. A **674**, 249 (2000).
44. M. Nikipelov *et al.*, Phys. Lett. B **540**, 207 (2002).
45. B. J. Ver West, R. A. Arndt, Phys. Rev. C **25**, 1979 (1982)
46. K. Tsushima, S. W. Huang, A. Faessler, J. Phys. G **21**, 33 (1995); Phys. Lett. B **337**, 245 (1994).
47. P. Moskal *et al.*, Phys. Lett. B **482**, 356 (2000).
48. E. Ya. Paryev, Eur. Phys. J. A **5**, 307 (1999).
49. V. Koptev *et al.*, Eur. Phys. J. A **17**, 235 (2003).
50. S. Barsov *et al.*, Acta Phys. Pol. B **31**, 2159 (2000).